www.amlett.com, www.amlett.org, DOI: 10.5185/amlett.2012.8404 Published online by the VBRI press in 2013

Electrical properties of barium titanate dispersed silver sulphate

S. W. Anwane*

Department of Physics, Shri Shivaji Science College, Congress Nagar, Nagpur, India 440012

*Corresponding author. E-mail: Tel: (+91) 7122423432; Fax: (+91) 7122440955; E-mail: swanwane2000@yahoo.com

Received: 02 August 2012, Revised: 19 September 2012 and Accepted: 23 September 2012

ABSTRACT

Composite materials which are heterogeneous mixtures of two or more solid phases offer value added properties for device applications. When ion conducting Ag_2SO_4 is dispersed with insulating $BaTiO_3$, enhanced electrical properties are observed along with improved surface morphology. The electrical properties have been derived from the Complex Impedance Spectroscopic studies. Arrhenius Plot, Concentration and Temperature dependent conductivity and activation energy have also been studied. The ionic transference number of the composite system remains unchanged on dispersion thereby retaining its category as Solid Ionic Conductor (SIC). Moreover, 30 Wt% $BaTiO_3$ dispersed in Ag_2SO_4 offers promisingly enhanced ionic conductivity and reduced activation energy of ion migration. This material has further scope for its utilization as a silver ion conductor in electrochemical applications like solid state batteries, gas sensors etc. The results obtained fit well in the established theories of composites.

Keywords: Barium titanate dispersed silver sulphate; fast ionic conductors; solid electrolyte; silver ion conductor; heterogeneous mixtures.

S. W. Anwane obtained Ph.D. degree from Nagpur University in 2000 and is working as Associate Professor in Physics at Shri Shivaji Education Society Amravati's SCIENCE COLLEGE, Congress Nagar, Nagpur. He has worked on Fast Ionic Conductor, Solid Electrolytes, Gas Sensors, Simulation. He has published books on Applied Physics, Electromagnetic Fields. He is recipient of Senior Research Fellowship of Council of Scientific & Industrial Research, New Delhi.

Introduction

Composite materials are heterogeneous mixtures of solid phases. The elaboration of composites offers a new degree of freedom in the search for advanced functional materials, because specific properties can to a certain degree be tailored by mixing appropriate phases. In the domain of solid state ionics, two routes can lead to improved solid ionic conductors: a search for new compounds and structures sustaining high levels of ionic conductivity or a modification of existing compounds, by heterogeneous or homogeneous doping. The latter involves homogenous dissolution of a certain amount of aliovalent dopant in the bulk of the ionic conductor M^+X^- in order to increase the concentration of mobile charge carriers according to bulk defect equilibrium. One example is the creation of additional vacancies by doping with cations of higher valence, such as D^{2+} in substitution of M^+, written in KroÈger-Vink nomenclature **[1-10]**:

$$DX_2 + 2M_M \rightarrow D_M^{\cdot} + V_M^{'} + 2MX \quad \text{.....} \quad (1)$$

Heterogeneous doping, on the contrary, involves mixing with a second phase with very limited solid solubility and the formation of defect concentration profiles in the proximity of interfaces. The deviations from local electrical neutrality (space charges) are a consequence of point defect equilibrium at interfaces [**11**]. Apart from the improvement

of the electrical properties, such as high conductivity and ionic transference number, the development of composite materials can also lead to better mechanical properties, such as better shock resistance or higher strength. Although composite materials can in principle contain many different phases, literature in the field of solid state ionics deals primarily with two-phase mixtures. In 1973, Liang [**12**] observed an enhancement of ionic conductivity by a factor of almost 50 in a composite material made from lithium iodide LiI, a compound with moderate Li ion conductivity at ambient temperature, and dispersed small alumina Al_2O_3 particles. The maximum lay around 40 vol% alumina. After this initial study, the conductivity enhancement in heterogeneous materials was confirmed for numerous ceramic composites, including dispersions of fine insulator particles in an ionic conductor matrix and mixtures of two different ionic conductors, with a major contribution by J. B.Wagner [**13**] and his group. The majority of study was made on monovalent cation conductors, such as lithium, silver and copper halides, the largest group being lithium compounds, given their importance in high energy density portable batteries. Besides Al_2O_3, other oxides, such as MgO, SiO_2, CeO_2, TiO_2 and ferroelectric $BaTiO_3$, were found to be effective second phases for ionic conductivity improvements.

More recently, the composite effect was also observed in ceramic anion conductors, such as lead or calcium fluoride, and even in inorganic solids with trivalent cation conductivity, like aluminum and rare-earths. The theory of ionic conductor composites, which is developed in the first part, highlights the importance of phase boundaries for the electrical properties. Boundaries can be transport pathways or transport barriers, given their modified core structure (core effects), and can affect the charge carrier distribution in the adjacent regions (space charge effects). Local deviations from electrical neutrality in the vicinity of interfaces were recognized long time ago in the electrochemistry of liquid electrolytes or in colloidal systems. Gouy [**14**] established the theory of the electrical double layer at the electrode-electrolyte interface in 1903 and Overbeek and co-workers [**15**] the electrostatic colloid theory in 1948. Lehovec [**16**] calculated in 1953 the defect distribution at the surface of ionic crystals and discussed the implications for ionic conduction. In 1972, Wagner [**17**] used the space charge layer concept to explain conductivity effects in two-phase materials with electronic conduction, such as metallic inclusions in a semiconducting oxide or mixtures of two semiconducting oxides. After an attempt by Jow and Wagner in 1979 [**18**], Maier [**19, 20**] established the space charge layer theory of heterogeneous ionic conductors after 1984. Ceramic composites, which are mixtures of two crystalline inorganic phases, represent so far the most important group in solid state ionics, but a growing amount of work was recently devoted to glass-ceramic composites, obtained by partial crystallization of a glassy matrix, and polymer-ceramic composites, where an inorganic compound is dispersed in a polymer matrix. Agrawal and Gupta [**21**] reviewed composite solid electrolytes and gave an extensive list of systems reported in the literature.

Silver sulphate, a non-alkali metal sulphate, is an exception which shows high cationic conductivity in spite of the bigger size of Ag^+. It undergoes a structural phase transition from the high temperature highly conducting hexagonal α-phase to the low temperature moderately conducting orthorhombic β-phase at 416^{o}C. It attracted scanty attention until its potential application in SO_x (x=2, 3) galvanic sensors was proved [**22**]. Ever since the concept of using a metal/metal sulphate reference electrode in solid electrochemical gas sensors has evolved, it has attracted a great deal of attention. It exhibits many advantages over other sulphate-based [**23**] solid electrolytes in engineering SO_2 gas sensors like: (*i*) coexistence of Ag−O−S phase in Ag/Ag_2SO_4; (*ii*) equilibration of antagonist SO_4^{2-}(solid) with SO_2/SO_3 (gas); (*iii*) invariance of high ionic conductivity over the SO_x environment, etc. [**24-32**].

The present work aims at dispersing insulating $BaTiO_3$ in silver ion conducting Ag_2SO_4 to study the properties of the two phase composite system. The materials with high purity blended appropriately and prepared by solid state sintering method. The electrical properties of the mixtures have been studied in detail. All the specimens prepared have been thoroughly characterized by Complex Impedance Spectroscopic studies at different temperatures. The temperature and concentration dependence of conductivity and activation energy have been studied and analyzed. At 30 Wt% $BaTiO_3$ dispersed in Ag_2SO_4 offers promisingly enhanced ionic conductivity and reduced activation energy of ion migration. The improved surface morphology is also an added feature for device application. This material is potential for its utilization as a silver ion conductor in electrochemical applications like solid state batteries, gas sensors etc. The conductivity results obtained fit well in the established theories of composites.

Theory of ionic conduction in composites

Interfaces play an important role for the transport properties of polycrystalline and poly-phase (composite) materials. Given the anisotropy of boundaries, one has to distinguish between transport along and across interfaces. Enhanced ionic conduction along interfaces can be observed for two reasons. First, the interface core itself is a disordered region, where defect formation and migration energies are generally notably reduced. This leads to enhanced ionic transport within the interface core (grain boundary diffusion). However, core effects are generally small, given the reduced interface area in conventional microcrystalline materials. Some studies established the role of grain boundary diffusion in polycrystalline oxides, including NiO, Al_2O_3, MgO [**33**] or ZnO [**34**], but there seems to be no similar study in composite materials. Second, point defect and dopant interactions with interfaces, for example accumulation in the interface core (intrinsic and extrinsic interfacial segregation), induce concentration profiles of point defects in the regions adjacent to the interface in ionic materials (space charge layers). Only few quantitative studies exist on grain boundary segregation in oxides,including CaO-doped ZrO_2 [**35**], TiO_2 [**36**] and CeO_2 [**37**] and similar studies on phase boundaries in composite materials are even more difficult, from an experimental as well as a theoretical point of view. The concentration profiles of mobile charge carriers near

interfaces are a consequence of thermodynamic defect equilibrium.

Experimental

Synthesis

The initial ingredients Ag_2SO_4, $BaTiO_3$ with assay 99.99% were procured from Aldrich Chemicals (USA). These pre-dried initial ingredients with weight fractions $(100-x)Ag_2SO_4$:(x) $BaTiO_3$ (where x=0 to 50 weight%), were mixed in an agate mortar under acetone for 2 hrs so as to ensure homogenous mixing. This mixture was later heated (in translucent silica quartz ampoules) up to the melting point of the host matrix. This ensures the fusing of $BaTiO_3$ in to the molten state of host Ag_2SO_4 and subsequently cooled to room temperature. The ingots obtained from ampoules were pulverized to get a fine powder. The powder of each composition was pressed uni-axially using Specac make stainless steel die-punch at pressure of 3 tons/cm^2 to obtain pellet of dimension 9mm in diameter and 1-2 mm thick. Finally the pellets were sintered at 500^{o}C, well below the melting point of host matrix for fixed duration of an hour followed by slow cooling to room temperature.

Characterization

The prepared samples were characterized by X-ray powder diffraction (XRD) (Philips PW1700 diffractometer attached with PW 1710 controlling unit) using CuK_α radiation. The solid–solid phase transition temperature and the heat of transition were studied by Differential Scanning Calorimetry (DSC) using Mettler TA 4000, DSC 25 at a heating rate of 10^{o}C/min. The microstructures were examined with the help of Scanning Electron Microscope (SEM) (Cambridge 250 Mark-III stereoscan electron microscope). Using InfraRed (IR) spectroscopy, the stack plots of the samples were recorded in several spectral regions of interest using a Perkin-Elmer 983 IR spectrometer.

Measurements and conditions

For electrical characterization, the specimens obtained in the form of circular discs were used. Prior to spring loading of the pellets between silver electrodes, a good ohmic contact was ensured by applying silver paint (Aldrich USA) on both opposite parallel surfaces of the pellet, followed by baking at 200^{o}C for 2 hrs. Preceeding the impedance measurement, the spring-loaded sample was heated in a furnace to 510^{o}C for an hour to homogenize the charge carriers in the sample and simultaneously to remove the moisture content therein. Later, the temperature of the furnace was reduced in steps of 20^{o}C at the cooling rate of 2^{o}C/min. At the end of each cycle the sample was allowed to attain thermal equilibrium for a dwell time of 30 minutes using a Eurotherm 810 PID temperature controller. At the end of each dwell time, the real and imaginary parts of the impedance were measured as parametric functions of frequency in the range 5Hz–13MHz and temperatures from 510 to 100^{o}C during the cooling cycle using an HP 4192A IF impedance analyzer. The entire measurement system was properly shielded to avoid external electrical pickups. A stainless steel faraday cage prepared in domestic workshop was employed for this purpose.

The ionic transference number of the specimens was measured by Wagner's DC polarization method using a Keithley SMU 236 with cell configuration: *Ag/Electrolyte/Pt*

A good ohmic contact was ensured for above cell configuration by applying silver paint (Aldrich USA) on one side and platinum paint (Aldrich USA)on other surface of the pellet, followed by baking at 200^{o}C for 2 hrs. A small dc potential was applied across the above configuration to record current at zero and saturation time to obtain the ionic transference number.

$$t_i = \frac{\sigma_0 - \sigma_\infty}{\sigma_0} \quad \text{..... (2)}$$

The reproducibility of the impedance data and transference number was confirmed by repeating the measurement on freshly prepared samples.

Table 1. A comparison of experimental d and I/I_0 values with JCPDS data for (1-x) Ag_2SO_4: (x) $BaTiO_3$ for x=0, 10, 20.

x=10		x=20		JCPDS data		
d	I/I_o	d	I/I_o	d	I/I_o	Plane, Phases
4.6929	4	--	--	4.699	10	[111]β-Ag_2SO_4
3.9915	11	3.993	32	3.994	25	[220]β- Ag_2SO_4
3.1739	100	3.1738	71	3.177	70	[040]β- Ag_2SO_4
2.8781	20	2.872	38	2.873	100	[311]β- Ag_2SO_4
2.855	10	2.852	11	2.85	100	[110]$BaTiO_3$
2.6436	21	--	--	2.644	90	[022]β- Ag_2SO_4
2.4146	7	2.4633	46	2.421	30	[311]β- Ag_2SO_4
2.314	5	2.3144	31	2.328	30	[111]$BaTiO_3$
1.999	6	2.001	12	1.98	11	[242]β- Ag_2SO_4
-	-	2.0018	15	2.016	35	[200]$BaTiO_3$

Results and discussion

Structural characterization forms the very basis for understanding the structure correlated conduction mechanism. [**38-44**].

X-ray powder diffraction

The XRD pattern for all six systems (100-x) Ag_2SO_4: (x) $BaTiO_3$ for x=0, 10, 20, 30, 40, 50 were obtained at room temperature. A comparison of this data with the JCPDS, in the table given below suggests the presence of potential lines corresponding to standard lines corresponding to Ag_2SO_4 and $BaTiO_3$. Insubstantial variation in d values indicates that the second dispersed $BaTiO_3$ phase is insoluble. Moreover, the absence of any new lines rules out a chemical reaction of $Ag_2SO_4$with $BaTiO_3$. A comparison of experimental, d, and relative intensity values, I/I_0, with those of JCPDS data is given in **Table 1** for a couple of samples.

Differential Scanning Calorimetric (DSC) studies were carried out on all samples. It was observed that for *x*=0, 10, 20, 30, 40 weight % the DSC isotherms indicates fall in enthalpy with concentration of $BaTiO_3$. However, transition temperature remains almost invariant. A DSC isotherm for the sample *x*=0 is depicted in **Fig. 1**.

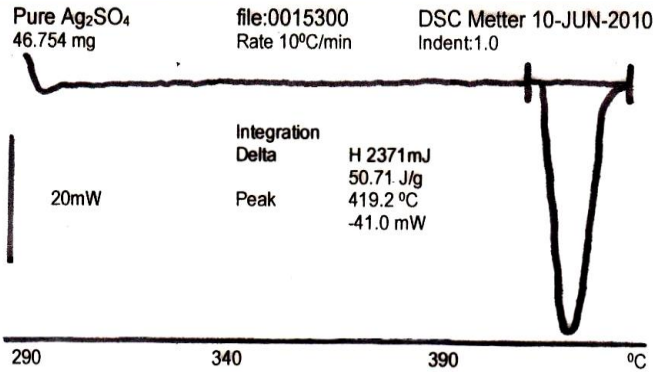

Fig. 1. DSC isotherm for pure Ag_2SO_4

Table 2. DSC data for (100-*x*)Ag_2SO_4:(*x*)$BaTiO_3$.

Sample Composition	J/gm	T °C
x=0	50.7	429.2
x =10	45.2	429.2
x =20	39.3	431.3
x =30	34.7	429.0
x =40	29.6	429.9

Table 3. DSC data for (100-*x*)Ag_2SO_4:(*x*)$BaTiO_3$.

Sample Composition	t_i
x=0	0.999
x =10	0.999
x =20	0.999
x =30	0.999
x =40	0.998

Differential scanning calorimetry (DSC)

The phase transition temperature and heat of transition obtained from the thermograms has been presented in **Table 2**.

Scanning electron microscopy (SEM)

The surface morphology of the $BaTiO_3$dispersed Ag_2SO_4 has been studied using Scanning Electron Microscopy (SEM). Fig. 2 representing microphotographs of (100-*x*)Ag_2SO_4:(*x*)$BaTiO_3$ with (*a*) *x*=0, (*b*) *x*=30 and (*c*) *x*=50 weight% reveals that the grain morphology of the host material is increasingly affected as the concentration of dispersed $BaTiO_3$ is increased. These results suggest that a complete two phase mixture is obtained in room temperature orthorhombic phase. This result supports the finding of XRD results.

Ionic transference number

The ionic transference number for *x*=0 to *x*=40 was carried out using Wagner's DC polarization method using Eq (2) has been presented in **Table 3**. This data shows that the ionic contribution to the conductivity of each composition does not depend upon the dispersion concentration of $BaTiO_3$ up to 40 wt%.

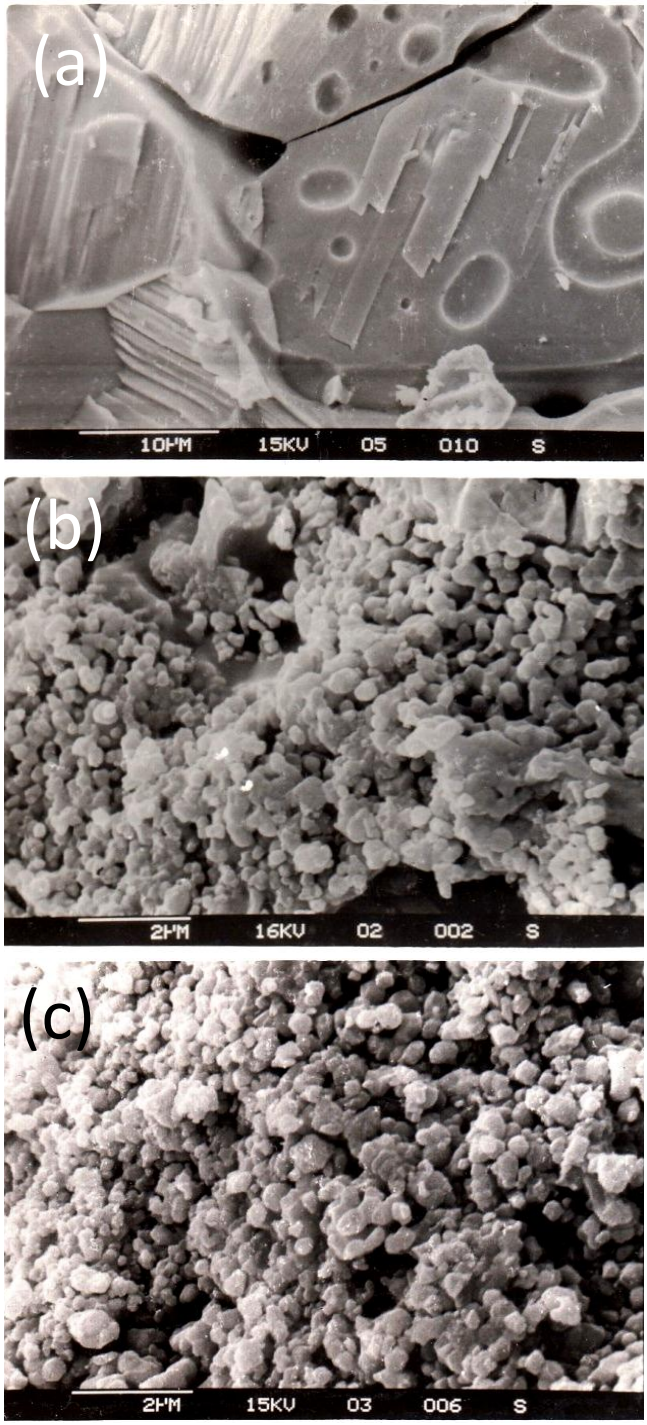

Fig. 2. SEM microphotographs for x=0, x=30, x=50.

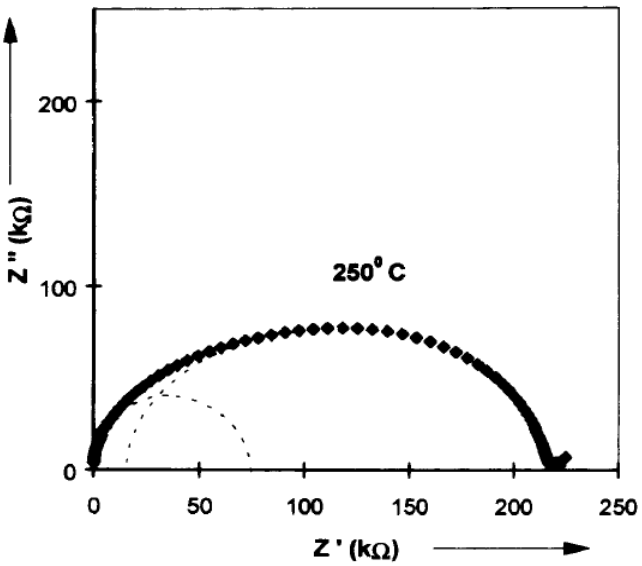

Fig. 3. Complex impedance plot for pure Ag_2SO_4 at 250 °C (the dotted line represents the best fit curve).

Impedance spectroscopy

The results of complex impedance spectroscopy are critically analyzed to find bulk properties by eliminating extraneous parameters such as electrode polarization and grain boundary. A distorted semicircular arc is observed for the pure sample **Fig. 3**. A closer look at this figure reveals that the distorted semicircular arc is a combination of two overlapping depressed semicircular arcs. However, there are two discernible semicircular arcs in the case of the rest of the samples.

Since the conductive silver coating on both the surfaces of the electrolyte acts as a reversible (non-blocking) electrode, no electrode polarization is reflected in the complex impedance plane. A non-linear least squares (NLS) fit method is used to ascertain the presence of two overlapping depressed semicircular arcs. In order to accomplish this, the complex impedance data acquired at a fixed temperature using a computer controlled HP 4192A IF impedance analyzer is fitted to the following equation using our software developed in *Turbo C*.

$$Z = Z(0) + \frac{Z(\infty)-Z(0)}{1+(j\omega\tau)^{\alpha}} \quad \text{..... (3)}$$

where $Z(0)$ and $Z(\infty)$ are limiting values of $Z(\omega)$ when ω varies from minimum to maximum, τ is relaxation time, α is empirical measure of departure from ideal Debye model. During the NLS fitting the sum of squares is minimized by unity weighting represented by,

$$S_i = (\Delta R_i)^2 + (\Delta I_i)^2 \quad \text{..... (4)}$$

where ΔR_i and ΔI_i are the real and imaginary fitting residuals. The presence of two overlapping depressed semicircular arcs is suggestive of the occurrence of two prominent conduction mechanisms simultaneously under the external perturbation ac signal. Various interpretations can be made in the impedance analysis in a polycrystalline ion conducting specimen; however, experimental impedance obviously contains major contributions from inter-grain and intra-grain ion migration [**45, 46**]. In order to have a more meaningful discussion, the voluminous impedance data obtained by following the above procedure are fit in using the equation,

$$f_p = f_0 e^{\frac{-E_m}{kT}} \quad \text{..... (5)}$$

The peak frequency of the complex impedance is,

$$\omega_{max} = 2\pi f_p$$
$$\frac{1}{\tau} = \frac{1}{RC} = \frac{\sigma}{\varepsilon\alpha\mu C}. \quad \mu = \mu_0 e^{\frac{-E_m}{kT}} \quad \text{..... (6)}$$

where μ is the cationic mobility, E_m denotes the migration enthalpy, μ_0 is proportional to the jump attempt frequency, and k and T are the Boltzmann constant and temperature in K. The frequency f_p derived from ω_{max} is an effective averaged hopping frequency of an ion. The effective pre-factor f_0 depends on the defect charge carrier density, C.

Table 4. Impedance data for (1-x) Ag_2SO_4: (x) $BaTiO_3$ for x=0, 10, 20, 30, 40, 50, 60 at 235°C(a) low frequency semicircle (b) high frequency semicircle.

(*a*)

x=	R_{b1}(kΩ)	α_1	f_{p1}	ln(f_{p1})	E_{a1}
0	6981	0.92	2638	12.142	0.61
10	6766	0.9	1800	11.4	0.551
20	2881	0.87	1778	10.463	0.412
30	2488	0.84	1258	10.707	0.435
40	713	0.87	3162	10.504	0.422
50	860	0.86	1778	10.664	0.43
60	212	0.81	4466	10.729	0.436

(*b*)

x=	R_{b2}(kΩ)	α_2	f_{p2}	ln(f_{p2})	E_{a2}
0	7241	0.87	3327	11.68	0.55
10	6800	0.87	1995	11.336	0.504
20	2786	0.85	2238	10.556	0.413
30	2243	0.85	1584	10.451	0.402
40	697	0.85	3700	10.571	0.415
50	760	0.88	2511	10.797	0.43
60	582	0.86	1600	10.885	0.435

The process of ion migration through the sample involves the activation energy for migration of ions across the grain boundaries, E_{a2} (obtained from the semicircle corresponding to high frequency) and that for migration of ions within grain (intra-grain), E_{a1} (obtained from the semicircle corresponding to low frequency). Evidently, the partial replacement of the host Ag^+ by dopant cations within the grain alters the local environment leaving the grain boundary undisturbed. This alteration in the local environment modifies the activation enthalpy for intra-grain

ion migration, whereas that for inter-grain conduction remains invariant [**47, 48**].

In the complex impedance plot, real and imaginary impedance has been plotted as a parametric function of frequency. The bulk resistance, peak frequency, depression of semicircle in complex impedance plot due to intergrain and intragrain ion migration process are presented in **Table 4**.

The variation in activation energies E_{a1} and E_{a2} arising from intergrain and intragrain processes are plotted as a function of $BaTiO_3$ concentration depicted in **Fig.4**. Around 30 wt% concentration offers minimal activation energy for ion migration.

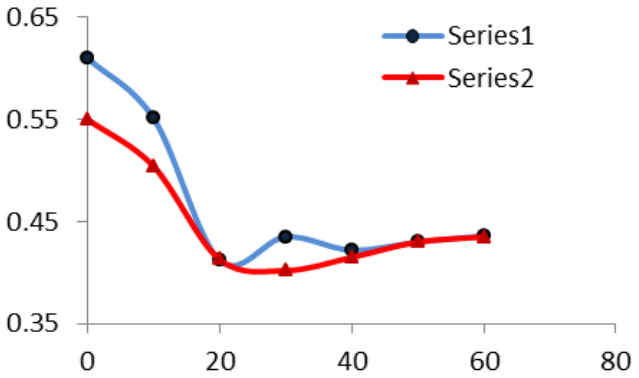

Fig. 4. Variation of E_{a1} and E_{a2} with concentration of $BaTiO_3$.

Ionic conductivity

The generalized perception of Arrhenius theory of the effect of temperature on the reaction rate (ion diffusion) originated from its effect on the equilibrium constant. It is known that:

$$\frac{d\ln(K)}{d\frac{1}{T}} = -\frac{H}{R} \quad \ldots\ldots\ldots\ldots (7)$$

where K is an equilibrium constant, R is the gas constant, and H is the heat of reaction. The equilibrium constant is $\frac{k_1}{k_2}$, where k_1 and k_1 are the rate constants for the forward and reverse reactions respectively. Thus, we obtain;

$$\frac{d\ln(k_1)}{d\frac{1}{T}} - \frac{d\ln(k_2)}{d\frac{1}{T}} = -\frac{H}{R} \quad \ldots\ldots\ldots\ldots (8)$$

Arrhenius recognized that the last equation could be conveniently divided into two parts, each having the form of:

$$\frac{d\ln(k)}{d\frac{1}{T}} = -\frac{E}{R} \quad \ldots\ldots\ldots\ldots (9)$$

where E is referred by Arrhenius as representing the energy difference between the reactants and the activated species. The term E is, therefore, called the activation energy. Taking E as a constant the last equation (9) can be integrated to yield:

$$\ln(k) = \ln(A) - \frac{E}{RT}$$

where $\ln(A)$ is the constant of integration. This equation can be converted to:

$$k = Ae^{-\frac{E}{RT}} \quad \ldots\ldots\ldots\ldots (10)$$

This form of equation (10) is the most widely adopted form of the Arrhenius equation. The temperature dependent ionic conductivity in all specimens is governed by Arrhenius equation can be expressed as equation (11);

$$(\sigma T) = (\sigma T)_o exp\left(\frac{E_a}{2KT}\right) \quad \ldots\ldots\ldots\ldots (11)$$

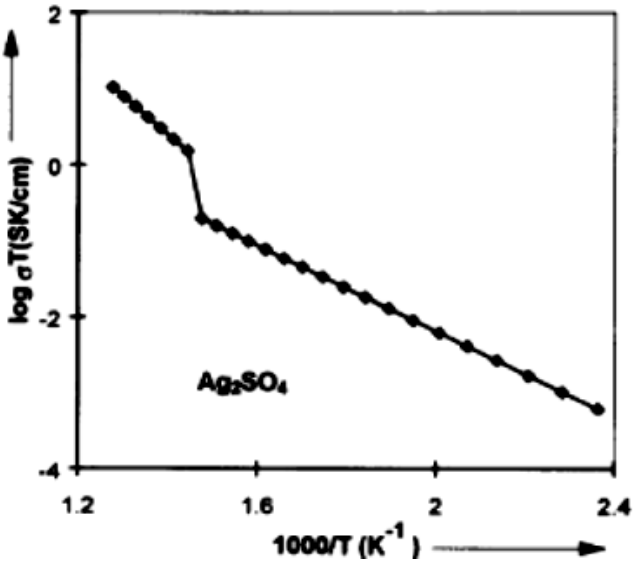

Fig. 5. Arrhenius plot for pure Ag_2SO_4 in α and β phases.

Table 5. Conductivity data in orthorhombic phase at 250°C.

Composition	log(σ)	$\log(\sigma T)_o$	E_a
x=0	-4.750	3.457	0.569
x=10	-4.249	3.330	0.503
x=20	-3.878	3.264	0.458
x=30	-3.610	3.139	0.417
x=40	-3.521	3.180	0.412
x=50	-3.395	3.003	0.381
x=60	-4.061	2.743	0.423

The pre-exponential factor $(\sigma T)_o$ in the above equation (which is appearing out of constant of integration) is related to the frequency of ionic collisions in the collision theory and to the entropy term in the transition state theory. The equation governs forward and reverse reaction contributing to ionic conductivity (σT) and predomination of each other. Arrhenius plots for all the compositions are found to obey the Arrhenius law (11) in both the α and β phases (as an example, **Fig. 5**. Arrhenius plot for pure Ag_2SO_4 in α and β phases depicts this behaviour for the host Ag_2SO_4).The observed change in slope at 416°C with an order of magnitude jump in conductivity in the case of pure Ag_2SO_4 accounts for the orthorhombic β to hexagonal α phase transition, **Fig. 5**. The magnitudes of the

conductivities (2.22×10^{-5} S/cm at 250°C and 3.4×10^{-3} S/cm at 440°C) and the transition temperature (416°C) are in close agreement with earlier reports [**49-52**]. **Table 5** presents the conductivity σ, pre-exponential factor $(\sigma T)_o$, activation energy for ion migration E_a for entire series of the samples under study in low temperature orthorhombic phase.

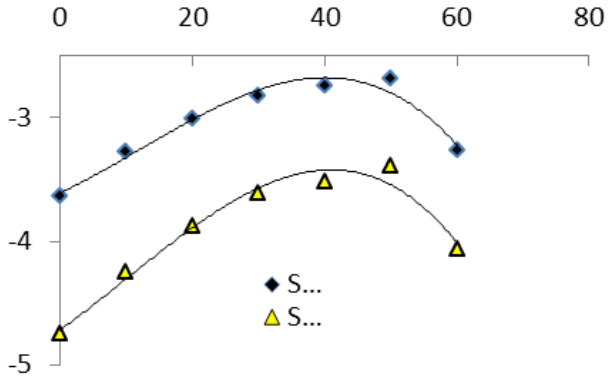

Fig. 6. Concentration dependent conductivity.

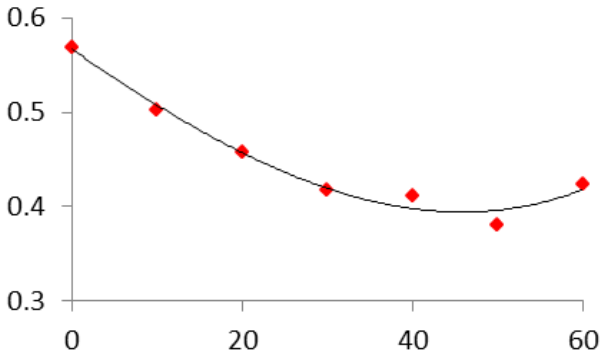

Fig. 7. Concentration dependent activation energy for ion migration.

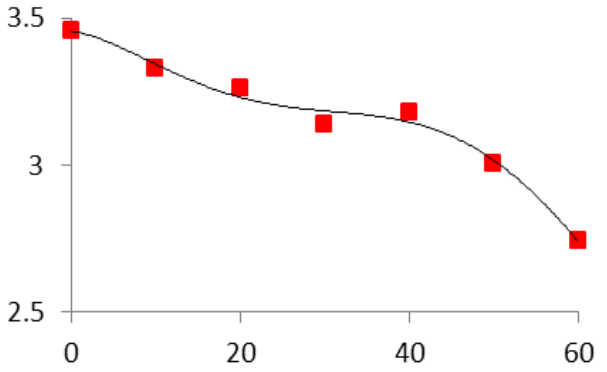

Fig. 8. Concentration dependent pre-exponential factor.

The concentration dependent trend in **Fig. 6** suggests that the composite solid electrolyte offers highest conductivity at *x*=40 wt%. Moreover, the activation energy required in the process of ion migration offers minima for 40 wt% $BaTiO_3$ dispersed in Ag_2SO_4. **Fig. 7** depicts the concentration dependent variation of activation energy. When the conductivity data is fit in Arrhenius equation (11), the pre-exponential factor arising out of line fitting offers a critical value at *x*=40wt% as shown in **Fig. 8**.

Space charge layer model

The fundamental concept is that ions can be trapped at the interface core. (This process is equivalent to a segregation phenomenon.) The counter species, in general, a trapped ion vacancy, is then accumulated in the adjacent space charge regions. Driving force is the chemical affinity of a second phase to the trapped ion. For example, "basic" oxides present many nucleophilic hydroxide surface groups, which can attract and fix cations. The space charge layer concept is a natural extension of volume defect thermodynamics, which takes the defect equilibrium at grain or phase boundaries into account [**2, 10, 11**]. Assuming an ionic solid M^+X^- with Frenkel disorder, the bulk defect equilibrium:

$$M_M + V_i = M_i^{\circ} + V'_M \quad \ldots\ldots\ldots\ldots (12)$$

is established between metal interstitials M_i and metal vacancies V'_M.

The Frenkel equilibrium constant reads:

$$K_f = [M_i][V'_M]\exp(-\Delta_f G^o/kT) \quad \ldots\ldots\ldots\ldots (13)$$

where the square brackets represent small defect concentrations and $\Delta_f G^o$ is the standard Gibbs free energy of formation of Frenkel defects.
The trapping of metal ions at interface sites can be written:

$$M_M + V_S = M_S^{\circ} + V'_M \quad \ldots\ldots\ldots\ldots (14)$$

here, V_S and M_S° are respectively an empty interface site and a metal ion trapped at an interface site. Supplementary metal vacancies are created in the adjacent space charge regions and, if the defect equilibrium is established locally, the number of interstitials is reduced because of the coupling Frenkel constant.

At equilibrium, the electrochemical potential of charged species, such as metal vacancies, is constant across an interface, but the chemical potential changes. For a diluted system, the local electrochemical potential $\eta(x)$ can be written:

$$\eta(x) = \mu(x) + z_i F\phi(x) \quad \ldots\ldots\ldots\ldots (15)$$

where $\phi(x)$ is the local electrical potential, z_i the defect charge and F Faraday's constant. The local chemical potential $\mu(x)$ is related to the molar concentration of defect $[i]$ (R is the universal gas constant).

$$\mu(x) = \mu^o + RT\ln[i](x) \quad \ldots\ldots\ldots\ldots (16)$$

The standard term μ^o contains concentration independent entropy and energy parameters. The equilibrium condition is:

$$d\eta(x) = 0 = d\left(RT\ln[i](x) + z_i F\phi(x)\right) \quad \ldots\ldots\ldots\ldots (17)$$

so that the monotonous defect concentration profile in the space charge region can be expressed as:

$$[i](x)/[i]_\infty = exp[-z_i F(\phi(x) - \phi_\infty)/RT] \quad \ldots\ldots\ldots\ldots (18)$$

The bulk concentration is a function of $[i]_\infty$ temperature, chemical potential and doping. The local concentration in the space charge region $[i](x)$ depends on the difference between the bulk and the local electrical potential, ϕ_∞ and $\phi(x)$. For $\phi(x) > \phi_\infty$, the concentrations of all negative defects are raised by the exponential factor, while those of the positive defects are reduced by the same factor and vice versa for $\phi(x) < \phi_\infty$.

The variation of defect profiles is observed over a distance approximately twice the Debye length λ, that is conveniently defined, like in semiconductor and liquid electrolyte theory, with respect to the bulk defect concentration $[i]_\infty$ ($\varepsilon\varepsilon_o$ is the dielectric permittivity) [10]:

$$\lambda^2 = \varepsilon\varepsilon_o RT/(2z_i^2 F^2 [i]_\infty) \quad \ldots\ldots\ldots\ldots (19)$$

Space charge effects are pronounced at reduced temperature, due to the low bulk defect concentrations. If the majority charge carriers are accumulated in the space charge regions, a considerable conductivity enhancement may result; given that a vacancy mechanism is observed in most solid ionic conductors at reduced temperature (extrinsic domain), ion trapping can lead to a major enhancement of the ionic conductivity.

The conductivity contribution of a single interface (bi-crystal experiment) can be calculated analytically by integration of the conductivity profile from the interface to the bulk. The calculation of the conductivity of a two-phase mixture, for example an ionic conductor/insulator composite, requires simplifications of the distribution topology, because there exists a complex superposition of various transport paths by bulk and interfaces.

Ionic conductor/insulator composites

Maier assumed a three-dimensional network of percolating paths with simple cubic symmetry. All components perpendicular to the current direction cancel out, while the remaining components with mean specific conductivity $\sigma_i$are connected in parallel and can be combined to an "effective" volume fraction $\beta_i\varphi_i$, which contributes to the quasiparallel circuit. The correction factor β_i takes values between 0.2 and 0.7. Neglecting transfer resistances, it follows that the conductivity of the composite can be written:

$$\sigma = \sum \beta_i \varphi \sigma_i \quad \ldots\ldots\ldots\ldots (20)$$

The physical reason for the formation of continuous conduction paths is the nature of the interfacial interactions. In the case of composites with dispersed insulator particles, the small size of the insulator particles with respect to the ionic conductor grains contributes to formation of continuous particle mono-layers, resembling the wetting of grains by a liquid phase.

For a large enhancement, the conductivity of the space charge region is a function of the geometric mean of the carrier concentration in the bulk $[i]_\infty$ and in the first layer adjacent to the interface $[i]_0$.

$$\sigma_{SC} = z_i F \mu_i ([i]_0 [i]_\infty)^{1/2} \quad \ldots\ldots\ldots\ldots (21)$$

For cubic grains, the effective volume fraction of space charge regions can be written as:

$$\varphi_{(SC)} = \beta(3\varphi_A/r_A)2\lambda \quad \ldots\ldots\ldots\ldots (22)$$

where φ_A is the volume fraction of second phase with mean grain size r_A. If the contributions of the insulator phase and the interface core (boundary diffusion) are neglected and the definition of the Debye length, Eq.(9), is used, the conductivity of the composite can be written:

$$\sigma = (1 - \varphi_A)\sigma_\infty + \beta(3\varphi_A/r_A)(2\varepsilon\varepsilon_o RT[i]_0)^{1/2}\mu_i \quad \ldots\ldots (23)$$

The first term describes the bulk conductivity and takes into account that the ionic conductor is partly replaced by insulator in the composite.

Mixtures of ionic conductors

Conductivity anomalies in a miscibility gap were detected in mixtures of two solid ionic conductors with Frenkel disorder, such as AgBr-AgI [**53**] and AgCl-AgI [**54, 55**]. Here, a silver ion can not only pass from one ionic conductor AgX to the interface, but also into the space charge layer of the neighboring ionic conductor AgX':

$$Ag_{Ag}(AgX) + V_i(AgX') \rightarrow Ag_i(AgX') + V'_{Ag}(AgX) \quad \ldots (24)$$

In this way, the vacancy concentration is enhanced in one ionic conductor and the interstitial concentration in the other. Equivalently, this process can be described by a transfer of Ag_i or V'_{Ag} between the two ionic conductors. The situation is analogous to the contact potential formed between two electronic conductors. The redistribution of mobile ions is due to a difference of standard Gibbs free energies of defect formation. Knuth [**56**] illustrates the processes during establishment of contact equilibrium, concentration profiles and measured conductivities in the system AgBr-AgI [**57**]. At the contact between two ionic conductors with Schottky disorder, such as LiBr-LiI [**58**], large effects are not expected in absence of charge accumulation at the phase boundary.

Composites

The trapping effects can be particularly important in nanocrystalline materials, which present a very large interface density. If the grain size L of the ionic conductor, or more generally the distance between interfaces or extended defects, becomes comparable with the Debye length, the space charge regions overlap and the grains are charged throughout. In nanoceramics, the thermodynamic bulk defect concentrations are not reached and the thermodynamic standard potential becomes size-dependent. This is similar to the quantum size effect in solid state electronics. An additional increase of conductivity can be

expected in the accumulation case and described by a ``nano-size" factor as given by Maier:

$$g = \left(\frac{4\lambda}{L}\right)\left\{\frac{[i]_0 - [i]^*}{[i]_0}\right\}^{1/2} \quad \ldots\ldots\ldots\ldots (25)$$

$[i]^*$, is the defect concentration in the grain center. For a large effect, $= \left(\frac{4\lambda}{L}\right)$, and a grain size $L = 0.4\lambda$, the conductivity would be enhanced by a supplementary order of magnitude.

Charge layer concept

The space charge layer model takes an idealized view of the interface. A major assumption is that the bulk structure is maintained up to the atomic layer in contact with the interface core: the variation of the materials parameters is assumed to take the form of a step function (abrupt core-space charge layer model). A continuous variation in the property due to a structural adjustment and energy gradients is more realistic in some cases, but is also more difficult to implement in a quantitative model. Several other processes can lead to a change of ionic conductivity.

Conclusion

Interfaces allow a variety of optimization strategies for materials. Boundary effects on transport phenomena are of outstanding importance in ionic conductor composites: given their anisotropy, interfaces can act as transport pathways or transport barriers (core effect) and they can affect the charge carrier distribution in adjacent regions, due to defect segregation at the interface (space charge effect).

Given the reduced interface core area in conventional composites, the space charge effect is often more important for practical properties. The conductivity enhancement observed in composite materials can be at least qualitatively understood and in some cases even quantitatively described by simple analytical equations derived from space charge theory. Many other experimental observations are also consistent with the “abrupt core-space charge model". Space charge effects at interfaces between nano-crystalline inclusions and a glass matrix can also explain the conductivity enhancement in some glass-ceramic composites.

The material 70 Ag_2SO_4:30 $BaTiO_3$ offers improved electrical properties over pure silver suplphate in terms of higher ionic conductivity, low activation energy of ion migration without alteration in ionic transference number. The SEM photographs reveal improved grain contacts. This material may have higher potential for application as silver ion conducting solid electrolyte in batteries and sensors as it offers improved electrical and morphology.

Reference

1. Tiwari, A.; Mishra, A.K.; Kobayashi, H; Turner, P F; *Intelligent Nanomaterials* Wiley-Scrivener Publishing LLC, USA, **2012** ISBN 978-04-709387-99, 2012 **DOI**:http://www.amazon.com/Intelligent-Nanomaterials-ebook/dp/B007DIAF16
2. Kobayashi, H *Adv. Mat. Lett.* **2012**, 3(4), 265 **DOI**: 10.5185/amlett.2012.9001
3. Tiwari,A; Mishra, A.P.; Dhakate, S R.; Khan,R; Shukla, S.K. *Materials Letters* **2007** 61(23–24) 4587 **DOI:** http://dx.doi.org/10.1016/j.matlet.2007.02.076
4. Tiwari,A; Prabaharan,M; Pandey, R R; Li S *J INORG ORGANOMET POLYM MATER* **2010** 20(2) 380 **DOI:** 10.1007/s10904-010-9354-9
5. Barik, S K; Choudhary, R.N.P.; Singh, A.K. *Adv. Mat. Lett.* **2011** 2(6) 419 **DOI:** 10.5185/amlett.2011.2228
6. Das, P R; Pati, B; Sutar, B C; Choudhury, R.N.P.; *Adv. Mat. Lett.* **2012**, 3(1), 8-14 **DOI:** 10.5185/amlett.2011.4252
7. Parida, B. N.; Das, P R; Padhee, R; Choudhary, R. N. P. *Adv. Mat. Lett.* **2012**, 3(3), 231 **DOI:** 10.5185/amlett.2012.2321
8. Rawat, M.; Yadav, K. L.; Kumar,A; Patel, P.K.; Adhlakha,N; Rani,J; *Adv. Mat. Lett.* **2012**, 3(4), 286 **DOI:** 10.5185/amlett.2012.2322
9. Singh, N. K.; Kumar, P; Rai, R; Kholkin, A L; *Adv. Mat. Lett.* **2012**, 3(4), 315 **DOI:** 10.5185/amlett.2011.9305
10. KroÈger, F.A. *The Chemistry of Imperfect Solid*s 2nd Ed **1974**. **DOI:** http://www.worldcat.org/title/chemistry-of-imperfect-crystals-2-imperfection-chemistry-of-crystalline-solids/oclc/490295263
11. Maier J. *Prog. Solid St. Chem*. **1995** 23, 171. **DOI:**10.1016/0079-6786(95)00004-E
12. Liang, C.C.; *J. Electrochem. Soc.* **1973** 120, 1289. **DOI:** 10.1149/1.2403248
13. Padma Kumar, P.; Yashonath, S. *J. Chem. Sci.* **2006** 118(1) 135 **DOI:**:10.1007/BF02708775
14. Torrie,G. M.; Valleau, J. P. *J. Phys. Chem.*, **1982**, 86 (16), 3251. **DOI:** 10.1021/j100213a035
15. Verwey, J.W.; J.Th.; Overbeek G; *Theory of the Stability of Lyophobic Colloids* **1948** (Elsevier, New York). **DOI:** 10.1002/pol.1949.120040321
16. Lehovec, K.; *J. Chem. Phys.* **1953** 21, 1123. **DOI:** http://dx.doi.org/10.1063/1.1699148
17. Wagner C. *J. Phys. Chem. Solids* **1972** 33, 1051. **DOI:** http://dx.doi.org/10.1016/S0022-3697(72)80265-8,
18. Jow, T.; Wagner, J.B. *J. Electrochem. Soc.***1979** 126, 1963. **DOI:**10.1149/1.2128835
19. Maier, J. *J. Phys. Chem. Solids* **1985** 46, 309. **DOI:** 10.1016/0022-3697(85)90172-6,
20. Maier, J. *Nature Materials* 4, 805 - 815 (2005) **DOI:**10.1038/nmat1513
21. Agrawal, R.C.; Gupta, R.K. *J. Mater. Sci.* **1999** 34, 1131. **DOI:** 10.1023/A:1004598902146
22. Gauthier, M; Chamberland, A. *J. Electrochem. Soc.* **1977** 124, 1579. **DOI:** 10.1149/1.2133114
23. Ramaswamy, V; Vimalathithan, R M; Ponnusamy, V *Adv. Mat. Lett.* **2012**, 3(1), 29-33 **DOI:** 10.5185/amlett.2011.4240
24. Liu, H Y; Hupp, J T; Weave, M J *J. of Electroanal Chemy & Interfacial Electrochem* **1984** 179, 1-2, 219. **DOI:** 10.1016/S0022-0728(84)80290-9
25. Liu, S H; Hinnen, C; Huong, C; Tacconi, N R; Hoa, K M; *J of Electroanalytical Chem & Interfacial Electrochem* **1984** 176, 1–2, 325. **DOI:** 10.1016/S0022-0728(84)80327-7
26. Mari, C.M.; Beghi, M; Pizrini, S. *Sensors and Actuators B*, **1990**, 2, 51-55. **DOI:** 10.1016/0925-4005(90)80008-N
27. Singh, K; Anwane, S W; Bhoga, S S *Solid State Ionics* **1996** 86-87, 187. **DOI:** 10.1016/0167-2738(96)00120-8
28. Singh, K; Pande, S M; Anwane, S W; Bhoga, S S *App. Phy. A* **1998** 66, 205. **DOI:** 10.1007/s003390050657
29. Singh, K; Pande, S M; Bhoga, S S *Bull Mater Sci* **1995** 19(3) 237. **DOI:** http://www.ias.ac.in/jarch/bms/18/00000246.pdf
30. Anwane, S W; Anwane, R S *Adv. Mat. Lett.* **2012**, 3(2), 77. **DOI:** 10.5185/amlett.2012.1314
31. Anwane, S W *Adv. Mat. Lett.* **2012**, 3(3), 204. **DOI:** 10.5185/amlett.2012.4332
32. Singh K; Pande S M; Anwane S W; Bhoga S S *Bull. of Electrochem* **1996** 12 (11-12) 625.

DOI: 10.1007/BF02745557
33. Atkinson, A. *Solid State Ionics* **1988** 28±30, 1377. **DOI:** http://dx.doi.org/10.1016/0167-2738(88)90390-6,
34. Wuensch, B.J.; Tuller, H.L. *J. Phys. Chem. Sol.* **1994** 55, 975. **DOI:** http://dx.doi.org/10.1016/0022-3697(94)90117-1
35. Aoki, M.; Chiang, Y.M.; Kosacki, I.; Lee, J.R.; Tuller, H.L.; Liu, Y. *J. Am. Ceram. Soc.* **1996** 79, 1169. **DOI:** 10.1111/j.1151-2916.1996.tb08569.x
36. Ikeda, J.A.S.; Chiang, Y.M. *J. Am. Ceram. Soc.* **1993** 76, 2437 and 2447. **DOI:** 10.1111/j.1151-2916.1993.tb03964.x
37. Chiang, Wang, Lee *J Microscopy* **2001** 191-3,275 **DOI:** 10.1046/j.1365-2818.1998.00377.x
38. Yeh, N C; Fu, C C; Wei, J Y T; Vasquez, R P; Huynh, J; Maurer, S M; Beach, G; Beam, D A *J. Appl. Phys.* **1997** 81, 8,5499. **DOI:** 10.1063/1.364580
39. Jin, S; Tiefel, T H; McCormack, M; Fastnacht, R A; Ramesh, R; Chen, L H *Appl. Phys. Lett.* **1995** 66, 382. **DOI:** 10.1063/1.114220
40. Hwang, H Y; Cheong, S W; Radaelli, P G; Marezio, M; Batlogg, B *Phys. Rev. Lett.***1995** 75, 914. **DOI:** 10.1103/PhysRevLett.75.914
41. Moritomo, Y; Asamitsa, A; Tokura, Y; *Phys.Rev.B* **1995** 51, 16 491. **DOI:** 10.1103/PhysRevB.51.16491
42. Khazeni, K; Jia, Y X; Lu, L; Crespi, V H; Cohen, M L; Zettl, A *Phys. Rev. Lett.* **1996** 76, 2, 295. **DOI:** 10.1103/PhysRevLett.76.295
43. Ibarra, M R; Algarabel, P A; Marquina, C; Blasco, J; Garcia, J; *Phys. Rev. Lett.* **1995** 75, 3541. **DOI:** 10.1103/PhysRevLett.75.3541
44. Zhao, G M; Conder, K; Keller, H; Muller, K A *Nature* **1996** 381, 676. **DOI:** 10.1038/381676a0
45. Singh, K *Solid State Ionics* **1993** 66, 5. **DOI:** 10.1016/0167-2738(93)90021-T
46. Muccilloa, ENS; Kleitzb, M *J European Ceramic Society* **1996** 16(4) 453. **DOI:** 10.1016/0955-2219(95)00125-5
47. Chamola, A; Singh, H; Naithani, U C; *Adv. Mat. Lett.* **2011**, 2(2), 148 **DOI:** 10.5185/amlett.2010.11183
48. Sahoo, S; Pradhan, D K; Choudhary, R. N. P.; Mathur, B. K. *Adv. Mat. Lett.* **2012**, 3(2), 97 **DOI:** 10.5185/amlett.2011.4250
49. Liu, Q; Worrel, W L *Solid State Ionics* **1988** 28-30(2) 1668. **DOI**: 10.1016/0167-2738(88)90439-0
50. Weppner, W *Solid State Ionics* **1981** 3(4) 1. **DOI**: 10.1016/0167-2738(81)90044-8 12
51. Weppner, W *Solid State Ionics* **1981** 5 (3). **DOI**: 10.1016/0167-2738(81)90186-7 13
52. Weppner, W *Sens & Actu* **1987** 12(2) 107. **DOI**: 10.1016/0250-6874(87)85010-2
53. Shahi, K.; Wagner, J.B. *J. Solid State Chemistry* **1982** 42 (2)107 **DOI:** http://dx.doi.org/10.1016/0022-4596(82)90256-0
54. Lauer, U.;Maier, J.; Bunsenges, B *Phys. Chem.* **1992** 96(2), 111. **DOI:** 10.1002/bbpc.19920960202
55. Jamnika, J.; Maiera, J.; Pejovnik, S. *Solid State Ionics* **1995** 75, 51. **DOI:** http://dx.doi.org/10.1016/0167-2738(94)00184-T,
56. Knauth, P. *J. Electroceramics* **2000** 5:2, 111±125. **DOI:**www.mpi.stonybrook.edu/energy/IonicConductivity/ionic-cond-5.pdf
57. Shahi, K.;Wagner, J.B. *Solid State Ionics* **1981** 3/4, 295. **DOI:** http://dx.doi.org/10.1016/0167-2738(81)90101-6 Dalvi, A.; Shahi, K.; *Solid State Ionics* **2002** 148, 3-4, 431.
58. **DOI:** http://dx.doi.org/10.1016/S0167-2738(02)00083-8

